Analysis and Parameter Optimization of Start-Up Process for *LLC* Resonant Converter

Ruichang Zheng, Bangyin Liu, *Member, IEEE*, and Shanxu Duan, *Member, IEEE*

***Abstract*—There is a current spike in *LLC* resonant converter during start-up and frequency modulation method is adopted to limit the resonant current usually, which controls switching frequency decreasing from specific high frequency to steady-state frequency in exponential pattern with a time constant tau. However, it is hard to determine the crucial parameter of time constant of the exponential switching frequency sweep curve, due to the complexity in analyzing dynamic process of the converter. In this paper, the operation modes and characteristics under continued conductive mode and discontinued conductive mode are analyzed based on state-plane analysis and the boundary of two conductive modes is figured out. Then, the iteration calculation model of the *LLC* converter is proposed to predict the resonant current during start-up progress, and time constant of the existing soft start method is optimized using iteration algorithm. Using the proposed iterative design method, the current stress of *LLC* resonant converter is limited, as well as guaranteeing the response speed of output voltage.**

***Index Terms*—Current limiting, *LLC* resonant converter, start-up, state-plane analysis.**

I. Introduction

THE *LLC* resonant converter has become an optimal topology for high-efficiency and high-power density dc–dc converter, and there are many research works focusing on its analysis and design [1]–[5]. However, the characteristics of multiresonant element and nonlinearity make it difficult to obtain the accurate model of the *LLC* resonant converter; thus, precise analytical expression of the converter behavior is unavailable. Fundamental harmonic approximation [6] causes some kind of error, while the computer-assisted method needs to solve the transcendental equations [5].

Current shock is a common problem during start-up and load disturbance of *LLC* resonant converter, which may cause damage to semiconductor devices or unnecessary protection. Different methods are proposed to limit the peak current of the resonant tank. Yang *et al*. introduce three solutions to achieve over current limitation: increasing switching frequency, variable frequency control plus pulse width modulation control and modification of power stage with clamping diode, which provides only qualitative analysis [7].

Manuscript received August 12, 2014; revised October 11, 2014 and December 19, 2014; accepted December 26, 2014. Date of publication January 6, 2015; date of current version August 21, 2015. This work was supported in part by the Funds for International Cooperation and Exchange of the National Natural Science Foundation of China (51361130150). Recommended for publication by Associate Editor G. Moschopoulos.

The authors are with State Key Laboratory of Advanced Electromagnetic Engineering and Technology, School of Electrical and Electronic Engineering, Huazhong University of Science and Technology, Wuhan 430074, China (e-mail: huakezrc@hust.edu.cn; lby@mailhust.edu.cn; duanshanxu@hust.edu.cn).

Color versions of one or more of the figures in this paper are available online at http://ieeexplore.ieee.org.

Digital Object Identifier 10.1109/TPEL.2015.2389116

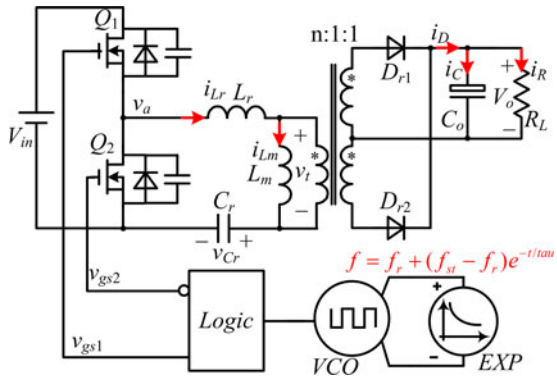

Fig. 1. *LLC* resonant converter with frequency modulation control for open-loop start-up.

Another current limiting circuit with an extra transformer and diodes to clamp the voltage of resonant capacitor is proposed in [8], which avoids the indeterminate setting point due to line and load condition in clamping diode method. Coordinated with frequency control, it shows effective improvement in limiting the shorted current. However, the analysis concerns on only short-circuit condition, and the cost of devices is increased.

The optimal trajectory control method in [9]–[11] uses graphical state trajectory analysis [11]–[14] to sketch out the feature of resonant capacitor voltage and inductor current in both state-plane and time domain. By sensing the output voltage, a soft start-up process is achieved without any current and voltage stress in the resonant tank [9]. The start-up time is ensured to be shortest by setting the converter to keep working at the maximum resonant current allowed. However, complex calculation in state trajectory control is time consuming and unavailable for low-cost MCU [15].

Frequency modulation control is the widely used and preferred choice to simplify the control strategy and save real-time calculation [16]–[18], which controls the switching frequency decreasing in exponential pattern or linear pattern from specific high frequency f_{st} to steady-state frequency f_r (e.g., $f = f_r + (f_{st} - f_r)e^{-t/tau}$), as shown in Fig. 1. The exponential pattern is easy to be carried out with a first-order filter and achieve more smooth transition of switching frequency. However, the trial-and-error method determining the frequency time constant *tau* is tedious [19], due to the lack of accurate analysis of dynamic process of the converter. In this paper, the start-up process is predicted based on the proposed iteration calculation model; then, the parameters of starting switching frequency and time constant are optimized to achieve the soft start-up with low current stress and fast response of output voltage.

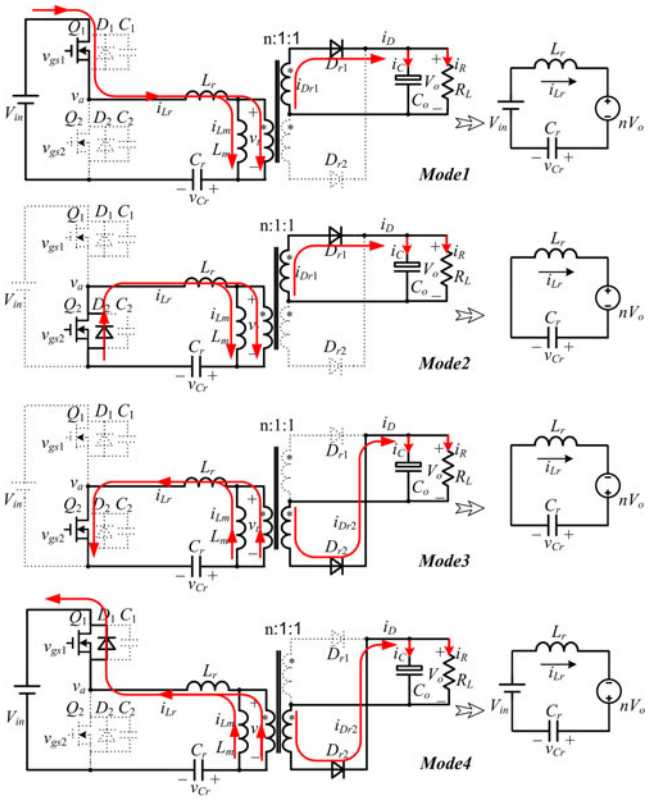

Fig. 2. Operation modes and equivalent circuits under CCM.

This paper is organized as follows. Section II introduces the basic state equations and solutions of the *LLC* converter with state-plane analysis. The boundary of operation modes is also obtained; Section III explains the principle to calculate the output voltage and resonant current with iteration operation, then the starting switching frequency and frequency time constant are optimized. Simulations and experiment results in Section IV show the validity of the analysis and design method.

II. State-Plane Analysis of the *LLC* Resonant Converter

A. State-Plane Analysis Under Continued Conductive Mode

Distinguishing different operation modes of the converter is important in iterative calculation of state variables. During start-up, the switching frequency decreases from specific high frequency to steady-state frequency, which means that switching frequency stays above the resonant frequency. The output capacitor behaves as a heavy load during start-up; thus, it can be assumed that output current of the rectifier diode is continuous conductive, and hence, the transformer is clamped to the output capacitor all the time. The voltage between magnetic inductor is $\pm nV_o$, while the voltage of neutral point of half bridge is V_{in} or 0 depending on the state of main switches, ignoring the charging and discharging time of the junction capacitor of main switches. Therefore, the operation modes can be divided to four modes as shown in Fig. 2. The main waveforms under continuous conductive mode are shown in Fig. 3.

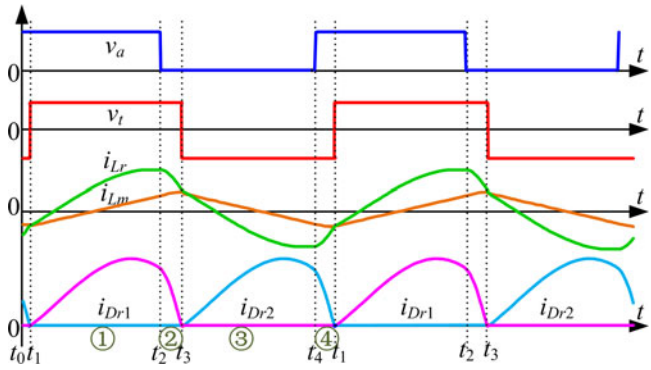

Fig. 3. Main waveforms under CCM.

The modes transition depends on the driving sequence and commutation of the rectifier diodes:

1) Mode1: D_{r2} freewheels to zero at t_1, D_{r1} begins to conduct, Q_1 keeps turning ON;
2) Mode2: Q_1 turns OFF at t_2, Q_2 turns ON, D_{r1} begins to freewheel;
3) Mode3: D_{r1} freewheels to zero at t_3, D_{r2} begins to conduct, Q_2 keeps turning ON;
4) Mode4: Q_2 turns OFF at t_4, Q_1 turns ON, D_{r2} begins to freewheel.

According to the equivalent circuit in Fig. 2, the state equation during Mode 1 is

$$\begin{cases} \dot{v}_{Cr} = \frac{1}{C_r} i_{Lr} \\ \dot{i}_{Lr} = -\frac{1}{L_r} v_{Cr} + \frac{1}{L_r}(V_{\text{in}} - nV_o) \end{cases} \tag{1}$$

where v_{Cr} and i_{Lr} are the resonant capacitor voltage and resonant inductor current.

Solving the differential equations,

$$\begin{cases} v_{Cr} = (V_{in} - nV_o) + I_{L0} Z_0 \sin \omega_0 t \\ +[V_{C0} - (V_{in} - nV_o)] cos \omega_0 t \\ i_{Lr} = I_{L0} \cos \omega_0 t - [V_{C0} - (V_{in} \\ -nV_o)] \sin \omega_0 t / Z_0 \end{cases} \tag{2}$$

where V_{C0} and I_{L0} are initial values of v_{Cr} and i_{Lr} at the beginning of the mode. Z_0 is the resonant impedance, $Z_0 = \sqrt{L_r/C_r}$. ω_0 is the natural frequency, $\omega_0 = 1/\sqrt{L_r C_r}$.

Moreover, (2) can be written as

$$\begin{aligned} &[v_{Cr} - (V_{\text{in}} - nV_o)]^2 + i_{Lr}^2 Z_0^2 \\ &= [V_{C0} - (V_{\text{in}} - nV_o)]^2 + I_{L0}^2 Z_0^2. \end{aligned} \tag{3}$$

It is obvious that the state trajectory of $(v_{Cr}, i_{Lr} Z_0)$ is circular arc, with the center $(V_{\text{in}} - nV_o, 0)$.

Solving the state equations of the other three equivalent circuits, it can be seen that the state trajectories of $(v_{Cr}, i_{Lr} Z_0)$

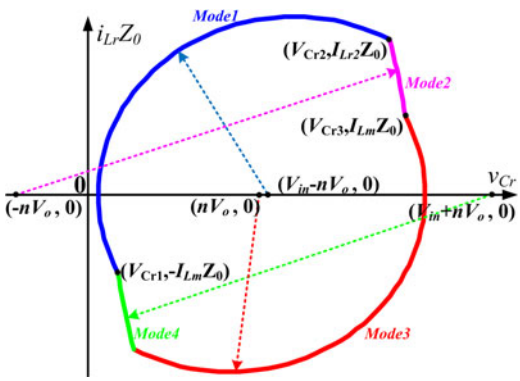

Fig. 4. State trajectory of resonant capacitor voltage and inductor current.

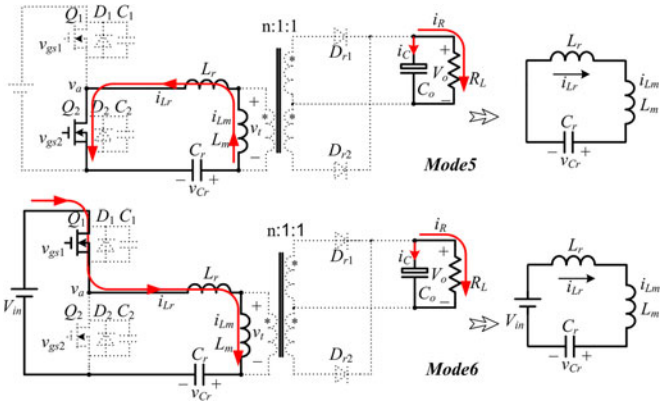

Fig. 5. Operation modes and equivalent circuits under DCM.

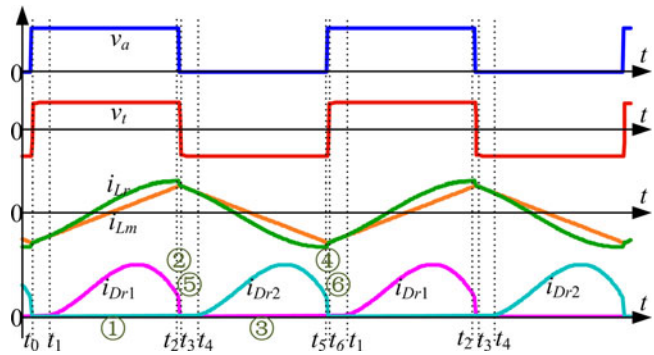

Fig. 6. Main waveforms under DCM.

are still circular arc, with different center point

$$\begin{cases} (v_{Cr}+nV_o)^2+i_{Lr}^2Z_0^2 \\ =(V_{C0}+nV_{oN})^2+I_{L0}^2Z_0^2 & |_{\text{Mode2}} \\ (v_{Cr}-nV_o)^2+i_{Lr}^2Z_0^2 \\ =(V_{C0}-nV_o)^2+I_{L0}^2Z_0^2 & |_{\text{Mode3}} \\ [v_{Cr}-(V_{in}+nV_o)]^2+i_{Lr}^2Z_0^2 \\ =[V_{C0}-(V_{in}+nV_o)]^2+I_{L0}^2Z_0^2 & |_{\text{Mode4}}. \end{cases} \tag{4}$$

The expression of center of arc $(x,0)$during four operation modes is

$$x=\begin{cases} V_{in}-nV_o|_{\text{Mode1}} \\ -nV_o \quad |_{\text{Mode2}} \\ nV_o \quad |_{\text{Mode3}} \\ V_{in}+nV_o|_{\text{Mode4}}. \end{cases} \tag{5}$$

Location of the center of arc and the state trajectory of $(v_{Cr},i_{Lr}Z_0)$ is shown in Fig. 4.

Thus, the state trajectory of $(v_{Cr},i_{Lr}Z_0)$ can be written in unified equations

$$\begin{cases} v_{Cr}-x=I_{L0}Z_0\sin\omega_0t+(V_{C0}-x)\cos\omega_0t \\ \quad =R\cos(\varphi-\omega_0t) \\ i_{Lr}Z_0=I_{L0}Z_0\cos\omega_0t-(V_{C0}-x)\sin\omega_0t \\ \quad =R\sin(\varphi-\omega_0t) \end{cases} \tag{6}$$

$$(v_{Cr}-x)^2+i_{Lr}^2Z_0^2=(V_{C0}-x)^2+I_{L0}^2Z_0^2=R^2 \tag{7}$$

where φ is angle of initial point $(V_{C0},I_{L0}Z_0)$ relative to the center of arc $(x,0)$

$$\varphi=\angle(V_{C0}-x,I_{L0}Z_0). \tag{8}$$

Conclusion can be drawn that the circular arc moves in a clockwise direction, since there is a negative sign before ω_0t in the unified equations.

B. Critical Condition for Continued Conductive Mode

The current flowing through rectifier diodes becomes discontinued conductive when the load becomes lighter, which will bring in two additional operation modes of the *LLC* converter and makes it more difficult to calculate the state variables during the start-up process. To ensure the validity of analysis and formula in Section III, the critical load condition is desired.

Two additional operation modes and main waveforms under discontinued conductive mode are shown in Fig. 5 and 6.

The boundaries and distribution of modes are illustrated by solving 9 to 13 mode equations in [20] and [21]. For the frequency region where switching frequency is higher than resonant frequency, a new method is presented as follow to obtain the boundary of operation modes, which avoids solving equations.

According to (6), assume that resonant current during t_1 and t_2 is

$$i_{Lr1}=I_{Lrp1}\sin(\omega_0t+\varphi_1). \tag{9}$$

In critical continued conductive mode, the slope of the resonant inductor current equals to the one of magnetic inductor at the inflection point of the exciting current

$$\omega_0I_{Lrp1}cos\varphi_1=\frac{di_{Lr1}}{dt}=\frac{di_{Lm}}{dt}=\frac{nV_o}{L_m}. \tag{10}$$

The resonant current equals to exciting current at t_0,

$$I_{Lrp1}\sin\varphi_1=I_{Lm}=\frac{nV_oT_s}{4L_m}. \tag{11}$$

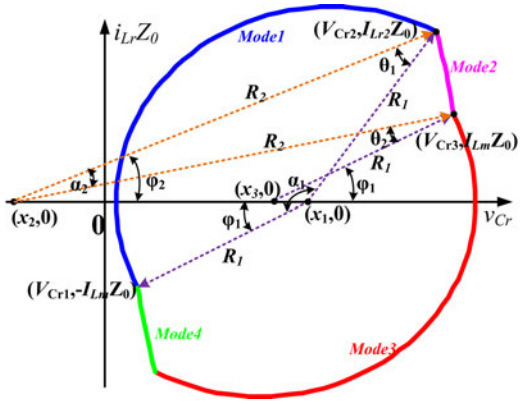

Fig. 7. Geometrical characteristic of the state diagram.

Therefore, the amplitude of resonant current is

$$I_{Lrp1} = \frac{nV_o}{\omega_0 L_m}\sqrt{1+\frac{\omega_0^2 T_s^2}{16}}. \tag{12}$$

In the state-plane diagram, as shown in Fig. 7, the radius of circular arc during Mode1 is

$$R_1 = I_{Lrp1}Z_0 = \frac{nV_o L_r}{L_m}\sqrt{1+\frac{\omega_0^2 T_s^2}{16}}. \tag{13}$$

According to the geometrical relationship

$$R_2^2 = (x_1 - x_2 + R_1\cos\varphi_1)^2 + R_1^2\sin^2\varphi_1 \tag{14}$$

$$R_2 = \frac{nV_o L_r}{L_m}\sqrt{\left(1+\frac{2L_m}{L_r}\right)^2+\frac{\omega_0^2 T_s^2}{16}}. \tag{15}$$

Thus,

$$\begin{cases} R_1 = \lambda_1 nV_o \\ R_2 = \lambda_2 nV_o \\ x_3 - x_2 = 2nV_o \end{cases} \tag{16}$$

where

$$\begin{cases} \lambda_1 = \dfrac{L_r}{L_m}\sqrt{1+\dfrac{\omega_0^2 T_s^2}{16}} \\ \lambda_2 = \dfrac{L_r}{L_m}\sqrt{\left(1+\dfrac{2L_m}{L_r}\right)^2+\dfrac{\omega_0^2 T_s^2}{16}}. \end{cases} \tag{17}$$

Considering all the lengths of three sides of the triangle B consist of $(x_3,0)$, $(x_2,0)$, and (V_{Cr3},I_{Lm}) are proportional to nV_o, thus vertex angle θ_2 of triangle B has no relationship with nV_o

$$\theta_2 = \arccos\left(\frac{\lambda_1^2+\lambda_2^2-4}{2\lambda_1\lambda_2}\right). \tag{18}$$

According to the geometrical relationship, vertex angle θ_1 of triangle A consist of $(x_1,0)$, $(x_2,0)$, and (V_{Cr2},I_{Lr2}) satisfies that

$$\theta_1 - \theta_2 = \pi - (\alpha_1+\alpha_2) = \pi - \omega_0 T_s/2. \tag{19}$$

Applying law of cosines to triangle A, the output voltage and normalized voltage gain M are

$$nV_o = \frac{V_{in}}{\sqrt{\lambda_1^2+\lambda_2^2-2\lambda_1\lambda_2\cos\theta_1}}. \tag{20}$$

$$M = \frac{2nV_o}{V_{\text{in}}} = \frac{2}{\sqrt{\lambda_1^2+\lambda_2^2-2\lambda_1\lambda_2\cos\theta_1}}. \tag{21}$$

The integral of symmetrical magnetic current i_{Lm} and the average value of output capacitor current i_C equals to zero during one conducting period of rectifier (equal to half a switching period) under steady state; thus

$$\begin{aligned} \int_0^{T_s/2} i_C dt &= \int_0^{T_s/2}(i_D - i_R)dt \\ &= \int_0^{T_s/2}(ni_{Lr} - ni_{Lm} - i_R)dt \\ &= n\int_0^{T_s/2} i_{Lr}dt - \frac{V_o T_s}{2R_L} = 0 \end{aligned} \tag{22}$$

where i_D is the sum of current of two rectifier diodes and i_R is the load current.

During one conducting period of rectifier, from t1 to t3

$$\int_0^{T_s/2} i_{Lr}dt = \int_0^{T_s/2} C_r\frac{dv_{Cr}}{dt}dt = C_r(V_{Cr3} - V_{Cr1}) \tag{23}$$

where V_{Cr1} and V_{Cr3} are the voltage of resonant capacitor at t1 and t3 separately, and

$$\begin{aligned} V_{Cr3} - V_{Cr1} &= 2R_1\cos\varphi_1 + 2nV_o - V_{\text{in}} \\ &= \frac{2nV_o Z_0}{\omega_0 L_m} + 2nV_o - V_{\text{in}} = \frac{L_m+L_r}{L_m}2nV_o - V_{\text{in}}. \end{aligned} \tag{24}$$

Therefore, the critical load resistor is

$$R_L = \frac{V_o}{2nC_r f\left(\frac{L_r+L_m}{L_m}2nV_o - V_{\text{in}}\right)}. \tag{25}$$

Normalizing switching frequency f with $f_r (f_r = 1/2\pi\sqrt{L_r C_r})$, the quality factor is

$$Q = \frac{Z_0}{R_{ac}} = \frac{\sqrt{L_r/C_r}}{8n^2 R_L/\pi^2} = \frac{\pi}{4}\left(1+\frac{L_r}{L_m}-\frac{1}{M}\right)f_n \quad (f_n \geq 1) \tag{26}$$

where R_{ac} is the ac equivalent load resistance, f_n is the normalized frequency, and $f_n = f/f_r$.

The relation curve of normalized voltage gain M, quality factor Q, and normalized frequency f_n under critical continued conductive mode is shown in Fig. 8, with which the conductive mode of *LLC* converter can be judged.

C. Equivalent Load During Start-Up

During start-up, the output voltage increases gradually while the current of output capacitor decreases. The output capacitor can be treated as dynamic load in parallel, which is defined as

$$R_C = \frac{V_o}{\bar{i}_C} = \frac{V_o\Delta t}{C_o\Delta V_o} = \frac{V_o T_s/2}{C_o\Delta V_o} \tag{27}$$

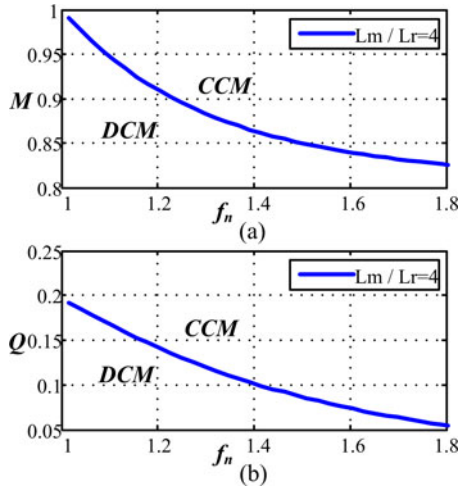

Fig. 8. Curves of (a) M versus $f_{\rm n}$ and (b) Q versus $f_{\rm n}$ under critical CCM.

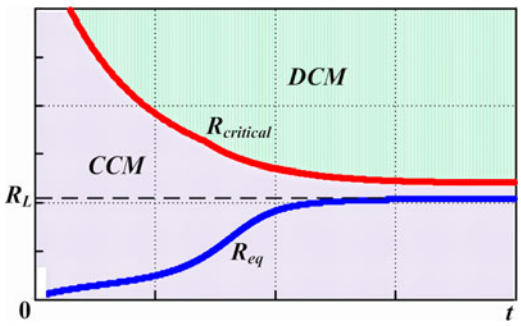

Fig. 9. Equivalent load and critical load during start-up.

where $\bar{i}_C$ is the average current of output capacitor during one switching period.

The output dynamic equivalent load is

$$R_{eq} = R_C // R_L = R_L / \left(1 + \frac{R_L C_o \Delta V}{V_o T_s / 2}\right). \tag{28}$$

Therefore, R_{eq} is equal to zero at the beginning and increases gradually until it reaches R_L. During the earlier time of starting-up, the output capacitor contributes to R_{eq} mainly, which makes it easier to enter the continued conductive mode. In the meantime, the switching frequency starts from high frequency, which means that the critical load for continued conductive mode is lighter at the beginning.

The output equivalent load is heavier than critical continued conductive load during all the start-up process if $R_L < R_{\rm critical}$, as shown in Fig. 9, which means that the *LLC* converter works under continued conductive mode all the time, then the analysis and calculation during start-up process can be simplified.

III. Start-Up Process and Parameter Optimization

According to the unified state equations, the radius and center of arc trajectory is closely relative to the output voltage. All state variables during start-up can be obtained if the output voltage is calculated out.

A. Calculation of Output Voltage

The rectifier current contributes to form the charging current of capacitor, subtracting the load current. Since the output capacitor is large enough, the output voltage during half a switching period can be treated constant, so does the load current. The incremental of output voltage during one conducting period of rectifier is

$$\Delta V_o = \frac{1}{C_o}\int_0^{T_s/2} i_C\,dt = \frac{1}{C_o}\int_0^{T_s/2} (i_D - i_R)dt. \tag{29}$$

According to (22) and (23)

$$\Delta V_o = \frac{nC_r(V_{Cr3} - V_{Cr1})}{C_o} - \frac{V_o T_s}{2R_L C_o}. \tag{30}$$

Assuming that

$$\begin{cases} i_{Lr1} = I_{Lrp1}\sin(\omega_0 t + \varphi_1)|_{\rm Mode1} \\ i_{Lr2} = I_{Lrp2}\sin(\omega_0 t + \varphi_2)|_{\rm Mode2} \end{cases} \tag{31}$$

φ_1 and φ_2 are initial phases relative to the center of arc $((x_1, 0)$and $(x_2, 0))$ at t_1 and t_2 separately, and

$$\begin{cases} I_{Lrp1} = \sqrt{(V_{Cr1} - x_1)^2/Z_0^2 + (-I_{Lm})^2} \\ I_{Lrp2} = \sqrt{(V_{Cr2} - x_2)^2/Z_0^2 + I_{Lr2}^2} \\ V_{Cr2} = I_{Lrp1} Z_0 \cos(\omega_0 t_{12} + \varphi_1) + x_1. \end{cases} \tag{32}$$

The inductor current satisfies that

$$\begin{cases} I_{Lrp1}\sin\varphi_1 = -I_{Lm} \\ I_{Lr2} = I_{Lrp1}\sin(\omega_0 t_{12} + \varphi_1) = I_{Lrp2}\sin\varphi_2 \\ I_{Lrp2}\sin(\omega_0 t_{23} + \varphi_2) = I_{Lm}. \end{cases} \tag{33}$$

The time between t_0 and t_2 equals to half a switching period,

$$t_{01} + t_{12} = T_s/2 \tag{34}$$

where t_{01} is the freewheeling time of the rectifier diode, which equals to $t_{23\_\rm last}$, the freewheeling time of the prior operation mode. Thus, all the variables are obtained, V_{Cr3} is then calculated, so as ΔV_o

$$V_{Cr3} = I_{Lrp2} Z_0 \cos(\omega_0 t_{23} + \varphi_2) + x_2. \tag{35}$$

The calculation of resonant current and output voltage during each of the operation modes is carried out with the iteration model shown in Fig. 10. Compared with numerical simulation method which needs 80–400 calculation nodes (corresponding to 10–50 ns simulation step under 250 kHz switching frequency) during each switching period to guarantee accuracy, the iteration calculation model needs only four calculation nodes during each switching period, corresponding to the ending moment of each operation modes. Therefore, the iteration calculation model is considerably simplified, time-saving and accurate, though it may take thousands of iterations before steady state is reached.

B. Peak Value of the Resonant Current

The peak value of the resonant current equals to the amplitude of resonant current when switching frequency is lower and equals to value of the resonant current at the end moment of

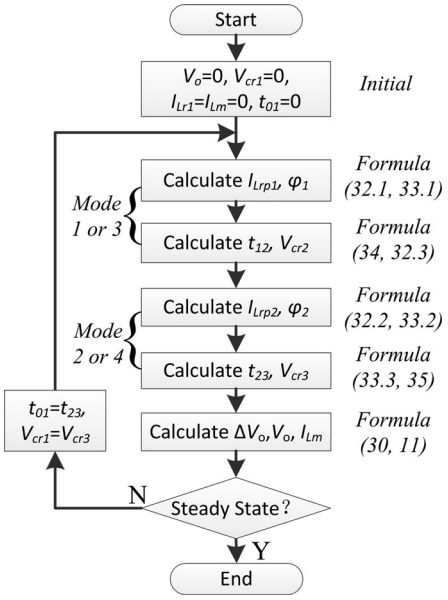

Fig. 10. Calculation of state variables with alternation model.

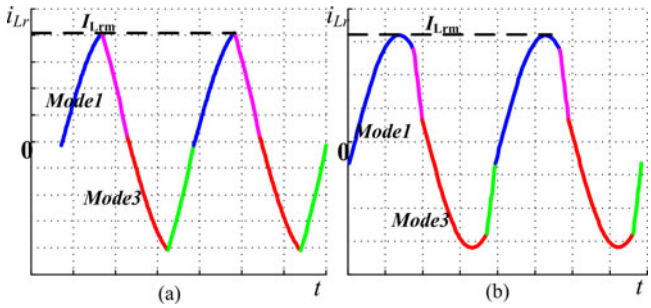

Fig. 11. Resonant inductor current under (a) high switching frequency and (b) low switching frequency.

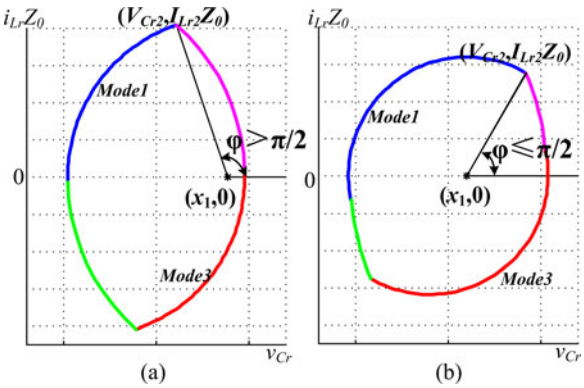

Fig. 12. State diagram under (a) high switching frequency and (b) low switching frequency.

Mode 1 and Mode 3 when switching frequency is higher, which is shown in Fig. 11.

With the plane diagram of $(v_{Cr}, i_{Lr}Z_0)$ in Fig. 12, it is easy to identify different status of the resonant current. The angel of $(V_{Cr2}, I_{Lr2}Z_0)$ relative to the center $(x_1, 0)$ is defined as φ, and

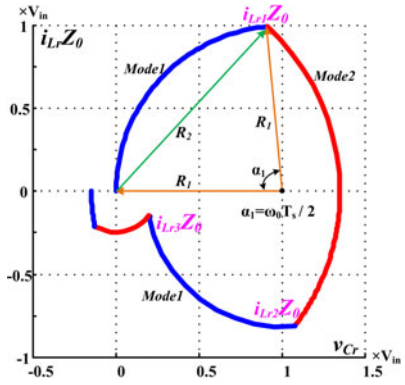

Fig. 13. State diagram at start-up moment with $f_n > 2$.

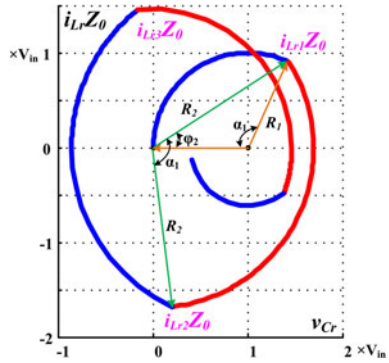

Fig. 14. State diagram at start-up moment with $1.5 < f_n \leq 2$.

the peak value of resonant current is

$$I_{Lrm} = \begin{cases} I_{Lrp1}\sin(\omega_0 t_{12} + \varphi_1), & \varphi < \pi/2 \\ I_{Lrp1}, & \varphi \geq \pi/2. \end{cases} \tag{36}$$

At the moment of start-up, the output voltage equal to zero; thus, $x_1 = x_4 = V_{in}$, $x_2 = x_3 = 0$, the operation modes decrease from four modes to two modes. The state diagram of (v_{Cr}, i_{Lr}) during the first two switching periods with an initial point $(0, 0)$ is shown in Fig. 13, where $R_1 = x_1 = V_{in}$. The radian of circular trajectory during each operation mode is defined as $\alpha_1 = \omega_0 T_s/2 = \pi/f_n$, the resonant current at the end of each mode is defined as i_{Lr1}, i_{Lr2}, i_{Lr3}, etc. A conclusion can be drawn from Fig. 13 that $i_{Lr3} < i_{Lr2} < i_{Lr1} < R_1/Z_0$ when $f_n > 2$, which means that $\alpha_1 < \pi/2$. Obviously, the peak value of the resonant current during first two switching period is

$$I_{Lrm} = i_{Lr1} = \frac{R_1}{Z_0}\sin\left(\frac{\omega_0 T_s}{2}\right) = \frac{V_{in}}{Z_0}\sin\left(\frac{\pi}{f_n}\right) \quad (f_n > 2). \tag{37}$$

The state diagram of (v_{Cr}, i_{Lr}) is shown in Fig. 14, when the start-up switching frequency decreases to $1.5 < f_n \leq 2$, which means that $\pi/2 \leq \alpha_1 < 2\pi/3$. It can be seen that $i_{Lr1} < R_1/Z_0 < i_{Lr3} < i_{Lr2} < R_2/Z_0$, thus

$$R_2 = 2R_1 \sin\left(\frac{\alpha_1}{2}\right) = 2V_{\text{in}} \sin\left(\frac{\omega_0 T_s}{4}\right)$$

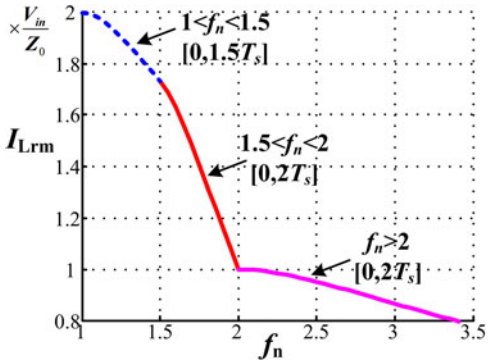

Fig. 15. Peak values of resonant current at start-up moment.

$$= 2V_{\text{in}} \sin\left(\frac{\pi}{2f_n}\right) \tag{38}$$

$$I_{Lrm} = i_{Lr2} = \frac{R_2}{Z_0}\sin(\alpha_1 - \varphi_2)$$
$$= \frac{R_2}{Z_0}\sin\left(\alpha_1 - \left(\frac{\pi}{2} - \frac{\alpha_1}{2}\right)\right)$$
$$= \frac{V_{\text{in}}}{Z_0}\sin\left(\frac{\pi}{f_n}\right) - \sin\left(\frac{2\pi}{f_n}\right) \quad (1.5 < f_n \le 2). \tag{39}$$

Similarly, the larger value of resonant current will occur during the following periods when the switching frequency continues to decrease, which is not concerned here because the starting frequency is much higher than the nominal one usually.

The relation between the peak values of resonant current with switching frequency at start-up moment is plotted in Fig. 15 at normalized coordinates. Obviously, higher starting switching frequency can reduce current shock at the start-up moment, but effect is weakened when $f_n > 2$. The required starting frequency can be determined with (37) and (39) according to the limit of resonant current at the start-up moment.

C. Optimization of Frequency Time Constant

Once the state variables during start-up process are calculated, the maximum value of resonant current is obtained, which can be compared with the current limit to verify the parameters of the converter. On the other hand, parameters can be optimized by iteration calculation to satisfy the current limitation.

For the *LLC* converter with certain circuit parameters operating with frequency modulation method, there are three factors affecting the maximum value of resonant current during start-up. The starting frequency is desired to be high enough to satisfy the current limit and considering the limit of speed of main switches, driving circuit, and controller. The final frequency is usually set to be the same with the frequency in steady state. The time constant controlling the decreasing speed of switching frequency is adjustable and critical. A short time constant will introduce an unacceptable current shock, in spite of applying the frequency modulation control.

Fig. 16 shows that a shorter time constant leads to much larger current shock than a longer one, both controlling the switching

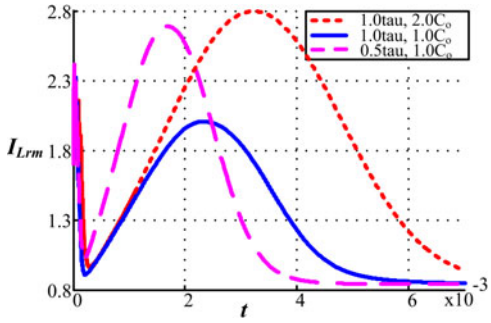

Fig. 16. Peak value of resonant inductor current during start-up.

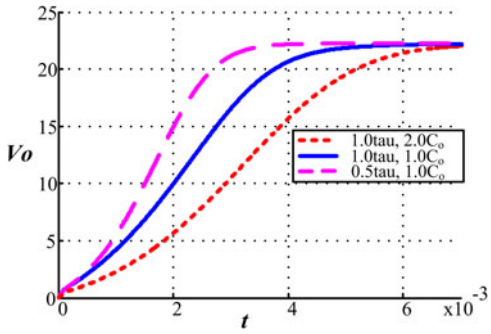

Fig. 17. Output voltage during start-up.

frequency decreasing from high frequency in an exponential function $f = f_r + (f_{st} - f_r)e^{-t/tau}$, where f_{st} is the starting switching frequency and tau is the frequency time constant. Larger output capacitor also draws larger current shock.

However, a longer time constant will slow down the response speed of the *LLC* converter and cause more settling time to build up the output voltage, as shown in Fig. 17.

The iteration design method can be used to figure out the optimal frequency time constant, as shown in Fig. 18. With the circuit parameters and an initial frequency time constant, the start-up process is calculated out and the peak value of the resonant current is obtained, which is compared with the current limit value to judge whether time constant satisfies the constraint. The time constant is tuned until it is large enough to limit the resonant current under the desired value. The optimized result is the minimum time constant, which satisfies the constraint of current limit and rapid response of the output voltage.

IV. Simulation and Experiment Results

A 100-W prototype was developed to verify the proposed iteration design method, with an input of 390 V and output of 24 V. The circuit parameters are shown in Table I.

The resonant frequency is $f_r = 1/2\pi\sqrt{L_r C_r} = 245\,\text{kHz}$, which equals to the frequency under steady state. The lowest switching frequency is set to be 150 kHz.

When output is shorted, the close-loop regulator will adjust the switching frequency to the lowest so as to boost up the output voltage. The amplitude of shorted resonant current is

$$I_{\text{shorted}} = \frac{4V_{in}}{\pi}\frac{1}{1/\omega_{\min}C_r - \omega_{\min}L_r}\frac{4}{3} = 3.01A \tag{40}$$

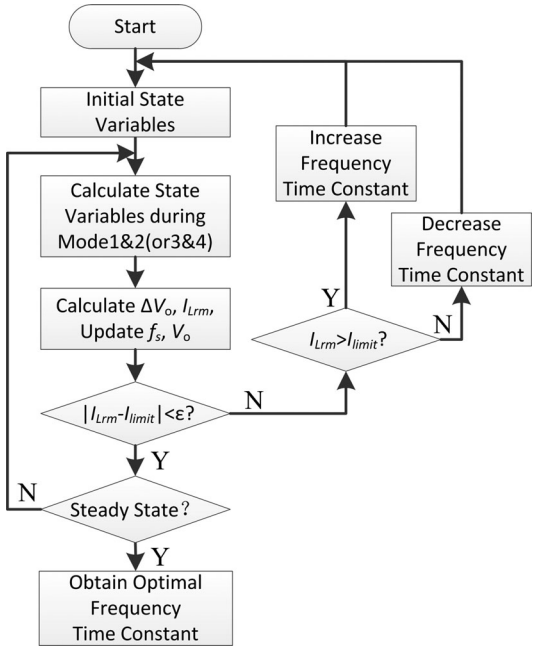

Fig. 18. Iteration algorithm for optimizing frequency time constant parameter.

TABLE I
PARAMETERS OF *LLC* RESONANT CONVERTER

Designed parameters	Values
Input Voltage (V_{in})	390 V
Output Voltage (V_o)	24 V
Resonant Inductor (L_r)	90 uH
Resonant Capacitor (C_r)	4.7 nF
Magnetic Inductor (L_m)	480 uH
Transformer Turns Ratio(n)	8:1:1
Output Capacitor (C_o)	1000 uF

where the coefficient 4/3 represents the effect of the harmonic and third-order harmonic of the square wave.

In order to avoid triggering the over current protection during start-up, the current limit of resonant current can be set to be 2.6 A.

The starting switching frequency is chose as 600 kHz, according to (37) and (39), considering the limit of speed of driving circuit and the controller LCS701 HG. Applying the proposed design method, the result of the optimized frequency time constant is 1.16 ms.

The output voltage and resonant capacitor current is compared in simulation result and calculated result, as shown in Fig. 19 and 20. The calculated output voltage fits with the simulation result well with maximum error of 1%, and the calculated amplitude of resonant current is almost identical with the simulation result.

The accurate prediction of resonant current and output voltage depends on knowing concrete circuit parameters; therefore, tolerance of the resonant components and output capacitor will affect the iteration calculation result of peak value of resonant current. Fig. 21 shows influence of different parameter tolerance on resonant current. About 10% mismatch of resonant inductance leads to 11–23% calculation error of the peak value of

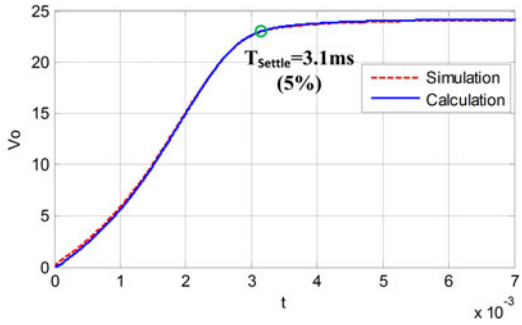

Fig. 19. Simulation waveform of output voltage compared with the calculated one during start-up.

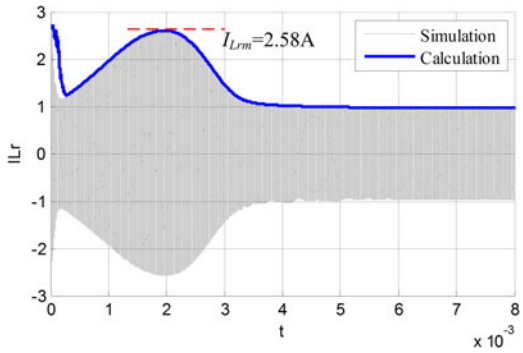

Fig. 20. Simulation waveform of resonant current compared with calculated envelope curve during start-up.

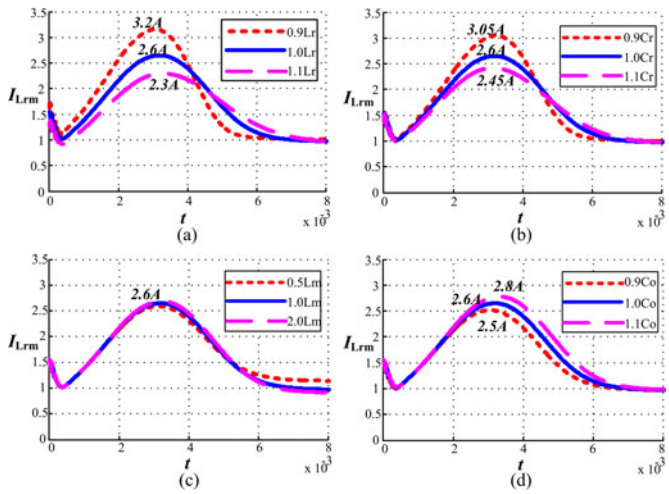

Fig. 21. Parameter tolerance influence on peak value of resonant current: (a) 10% resonant inductor mismatch. (b) 10% resonant capacitor mismatch. (c) 50% magnetic inductor mismatch. (d) 10% output capacitor mismatch.

resonant current, while 10% mismatch of resonant capacitance results in 6–17% calculation error. The magnetic inductance has little impact on the peak value but steady-state value of resonant current, and output capacitance has relatively slight influence on calculation with 4–8% error under 10% tolerance. As a result, it is suggested that the value of resonant inductor and capacitor be measured precisely so as to make accurate prediction of the resonant current.

The experimental result with full load and $\mathrm{tau} = 1.16$ ms is shown in Fig. 22(a). The experimental peak value of resonant

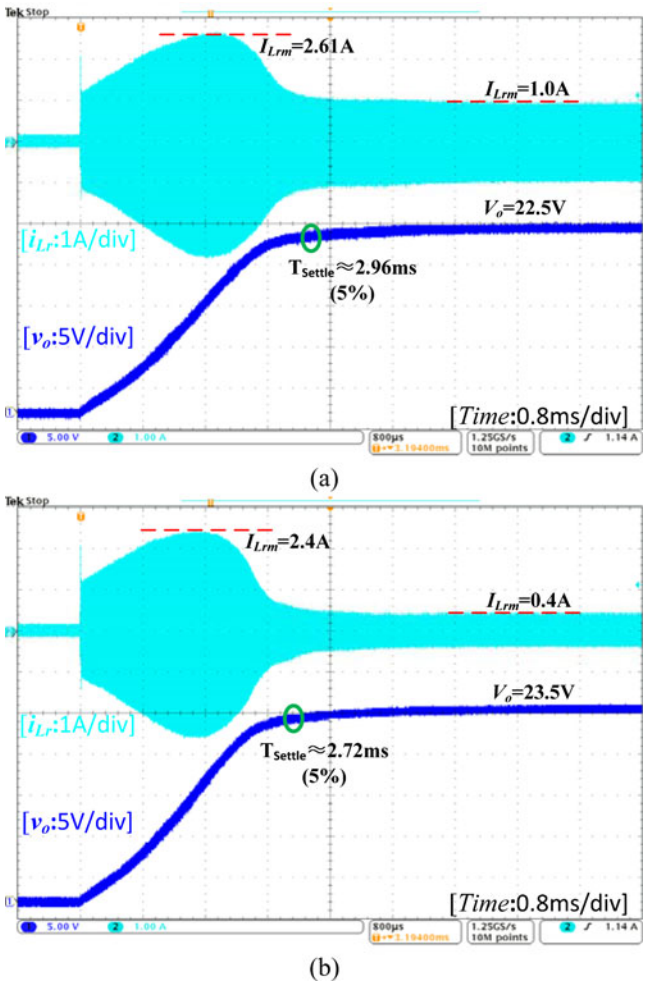

Fig. 22. Experimental waveform of output voltage and resonant current during start-up with $Co = 1000$ uF and $\mathrm{tau} = 1.16$ ms under (a) Full Load, $I_o = 4$ A, and (b) No Load, $I_o = 0$ A.

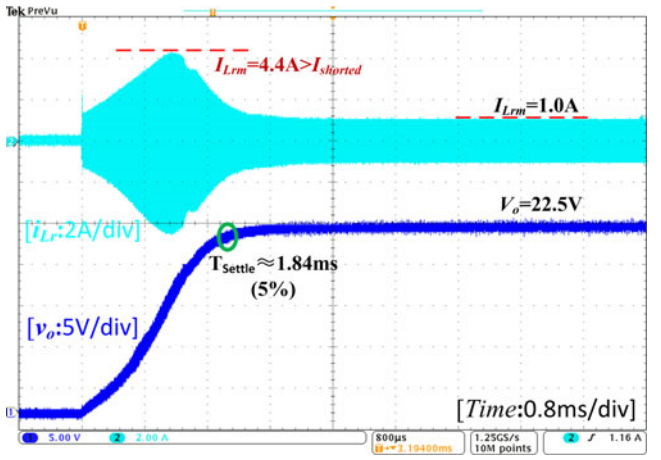

Fig. 23. Experimental waveform of output voltage and resonant current during start-up with $Co = 1000$ uF and $\mathrm{tau} = 0.5$ms.

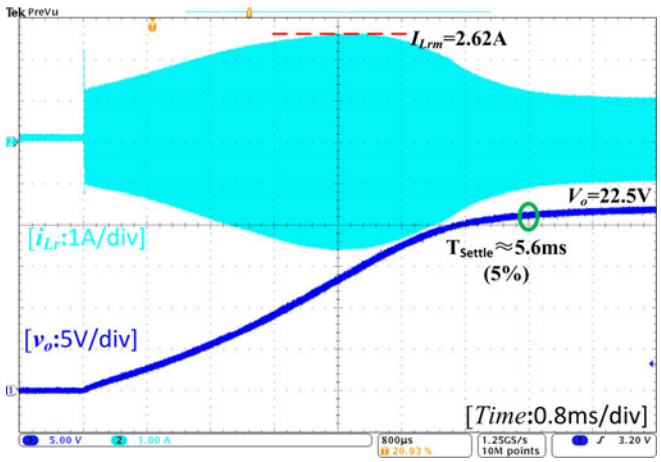

Fig. 24. Experimental waveform of output voltage and resonant current during start-up with $Co = 2000$ uF and $\mathrm{tau} = 1.94$ ms.

current is 2.61 A, and the settle time of the output voltage is 2.96 ms, which are closed to the calculation results. The current spike at the start-up moment is suppressed in the experiment because the dead time of drivers has more influence at higher starting frequency than lower steady-state frequency, and the dead time reduces the time for energy transportation as well as the current spike.

The experimental result with no-load and $\mathrm{tau} = 1.16$ ms is shown in Fig. 22(b). The peak value of resonant current is 2.4 A, a bit smaller than that under full load condition. In the meantime, the settle time of output voltage becomes a bit shorter (2.72 ms).

The experimental result with full load and an unoptimized frequency time constant ($\mathrm{tau} = 0.5$ ms) is shown in Fig. 23. The peak value of resonant current is 4.4 A, which exceeds the shorted resonant current, namely the over current protection value. Therefore, the optimization of frequency time constant is necessary.

Fig. 16 shows that larger output capacitor leads to larger current shock, thus longer frequency time constant is required to limit the resonant current. When the output capacitor increases from 1000 to 2000 uF, the optimal frequency time constant becomes 1.94 ms, according to iteration algorithm. Fig. 24 shows the experimental result with $\mathrm{Co} = 2000$ uF and $\mathrm{tau} = 1.94$ ms. The peak value of resonant current is limited to 2.62 A as expected, with longer setting time of the output voltage (5.6 ms).

V. Conclusion

Analysis of dynamic process of the *LLC* resonant converter in time domain and optimization of start-up frequency parameters has been presented in this study. The unified equations of different modes, as well as the boundary of continued conductive mode and discontinued conductive mode, are obtained based on state-plane analysis. The output voltage and peak value of resonant inductor current is calculated under continued conductive mode by iteration method, without any sensor in circuit. The impact on resonant inductor current with different output capacitor and frequency time constant is compared using the calculation model in time domain. Then, the optimal frequency time constant is optimized with iteration algorithm, which satisfies the resonant current limit and achieves a short start-up time. The state-plane analysis and iteration design method was verified to be accurate and directive in simulation and experiment.

REFERENCES

[1] B. Lu, W. Liu, Y. Liang, F. C. Lee, and J. D. Van Wyk, "Optimal design methodology for LLC resonant converter," in *Proc. IEEE Appl. Power Electron. Conf. Expo.*, 2006, pp. 1–6.

[2] X. Fang, H. Hu, F. Chen, U. Somani, E. Auadisian, J. Shen, and I. Batarseh, "Efficiency-oriented optimal design of the LLC resonant converter based on peak gain placement," *IEEE Trans. Power Electron.*, vol. 28, no. 5, pp. 2285–2296, May 2013.

[3] X. Fang, H. Hu, Z. J. Shen, and I. Batarseh, "Operation mode analysis and peak gain approximation of the LLC resonant converter," *IEEE Trans. Power Electron.*, vol. 27, no. 4, pp. 1985–1995, Apr. 2012.

[4] B. Yang, F. C. Lee, A. J. Zhang, and G. Huang, "LLC resonant converter for front end DC/DC conversion," in *Proc. IEEE Appl. Power Electron. Conf. Exp.*, 2002, pp. 1108–1112.

[5] R. Yu, G. K. Y. Ho, B. M. H. Pong, B. W. K. Ling, and J. Lam, "Computer-aided design and optimization of high-efficiency LLC series resonant converter," *IEEE Trans. Power Electron.*, vol. 27, no. 7, pp. 3243–3256, Jul. 2012.

[6] G. Ivensky, S. Bronshtein, and A. Abramovitz, "Approximate analysis of resonant LLC DC-DC converter," *IEEE Trans. Power Electron.*, vol. 26, no. 11, pp. 3274–3284, Nov. 2011.

[7] B. Yang, F. C. Lee, and M. Concannon, "Over current protection methods for LLC resonant converter," in *Proc. IEEE Appl. Power Electron. Conf. Expo.*, 2003, pp. 605–609.

[8] X. Xie, J. Zhang, C. Zhao, Z. Zhao, and Z. Qian, "Analysis and optimization of LLC resonant converter with a novel over-current protection circuit," *IEEE Trans. Power Electron.*, vol. 22, no. 2, pp. 435–443, Mar. 2007.

[9] W. Feng and F. C. Lee, "Optimal trajectory control of LLC resonant converters for soft start-up," *IEEE Trans. Power Electron.*, vol. 29, no. 3, pp. 1461–1468, Mar. 2014.

[10] W. Feng, F. C. Lee, and P. Mattavelli, "Simplified optimal trajectory control (SOTC) for LLC resonant converters," *IEEE Trans. Power Electron.*, vol. 28, no. 5, pp. 2415–2426, May 2013.

[11] W. Feng, F. C. Lee, and P. Mattavelli, "Optimal trajectory control of burst mode for LLC resonant converter," *IEEE Trans. Power Electron.*, vol. 28, no. 1, pp. 457–466, Jan. 2013.

[12] I. Batarseh, "State-plane approach for the analysis of half-bridge parallel resonant converters," *IEE Proc. Circuits, Devices Syst.*, vol. 142, no. 3, pp. 200–204, 1995.

[13] R. Oruganti and F. C. Lee, "Resonant power processors, part ii-methods of control," *IEEE Trans. Ind. Appl.*, vol. IA-21, no. 6, pp. 1461–1471, Nov. 1985.

[14] R. Oruganti and F. C. Lee, "Resonant power processors, Part I—state plane analysis," *IEEE Trans. Ind. Appl.*, vol. IA-21, no. 6, pp. 1453–1460, Nov. 1985.

[15] C. Fei, W. Feng, F. C. Lee, and Q. Li, "State-trajectory control of LLC converter implemented by microcontroller," in *Proc. Appl. Power Electron. Conf. Expo.*, 2014, pp. 1045–1052.

[16] Power Integrations. AN-55 HiperLCS Family Design Guide. (2011, Sep). [Online]. Available: http://www.powerint.com/sites/default/files/product-docs/an55.pdf

[17] ST Microelectronics. AN2450 LLC resonant half-bridge converter design guideline. (2014, Mar.). [Online]. Available: http://www.st.com/st-web-ui/static/active/en/resource/technical/document/application_note/CD00143244.pdf

[18] Texas Instrument, "LLC soft start by operation mode switching," U.S. Patent US8 018 740 B2, Sep. 13, 2011.

[19] Fairchild Semiconductor. (2007). AN-4151 Half-Bridge LLC Resonant Converter Design Using FSFR-Series Fairchild Power Switch. [Online]. Available: http://www.fairchildsemi.com/an/AN/AN-4151.pdf

[20] X. Fang, H. Hu, L. Chen, A. Amirahmadi, J. Shen, and I. Batarseh, "Operation analysis and numerical approximation for the LLC DC-DC converter," in *Proc. Appl. Power Electron. Conf. Expo.*, 2012, pp. 870–876.

[21] Z. Fang, T. Cai, S. Duan, and C. Chen, "Optimal design methodology for LLC resonant converter in battery charging applications based on time-weighted average efficiency," *IEEE Trans. Power Electron.*, to be published, DOI: 10.1109/TPEL.2014.2379278, 2015

Ruichang Zheng received the B.S. degree in electrical engineering from the Huazhong University of Science and Technology, Wuhan, China, in 2012. He is currently working toward the M.S. degree at the Huazhong University of Science and Technology.

His research interests include modeling and control of dc–dc converter, soft switching technique, and renewable energy applications.

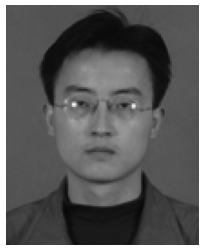

Bangyin Liu (M'10) received the B.S., M.S., and Ph.D. degrees in electrical engineering from the Huazhong University of Science and Technology (HUST), Wuhan, China, in 2001, 2004, and 2008,respectively.

He was a Postdoctoral Research Fellow with the Department of Control Science and Engineering, HUST, from 2008 to 2010, and is currently an Associate Professor with the School of Electrical and Electronics Engineering, HUST. His current research interests include renewable energy applications, soft switching converters, and power electronics applied to the power system.

Shanxu Duan (M'14) received the B.Eng., M. Eng., and Ph.D. degrees in electrical engineering from the Huazhong University of Science and Technology, Wuhan, China, in 1991, 1994, and 1999, respectively.

Since 1991, he has been a Faculty Member in the College of Electrical and Electronics Engineering, Huazhong University of Science and Technology, where he is currently a Professor. His research interests include stabilization, nonlinear control with application to power electronic circuits and systems, fully digitalized control techniques for power electronics apparatus and systems, and optimal control theory and corresponding application techniques for high-frequency pulsewidth-modulation power converters.

Dr. Duan is a Senior Member of the Chinese Society of Electrical Engineering and a Council Member of the Chinese Power Electronics Society. He was selected as one of the New Century Excellent Talents by the Ministry of Education of China in 2007. He also received the honor of "Delta Scholar" in 2009.